Leaky-Wave Radiations with Arbitrarily Customizable Polarizations Based on Spoof Surface Plasmon Polaritons

Meng Wang, Hui Feng Ma,* Wen Xuan Tang, Shi Sun, and Tie Jun Cui
State Key Laboratory of Millimeter Waves, School of Information Science and Engineering, Southeast University, Nanjing 210096, China

(Received 13 January 2019; revised manuscript received 18 June 2019; published 19 July 2019)

Spoof surface plasmon polaritons (SSPPs) can be converted to leaky-wave radiations by a spoof surface plasmon (SSP) waveguide with periodically modulated surface impedance, which is also known as a SSPP leaky-wave antenna (LWA). However, most of the reported SSPP LWAs can only radiate electromagnetic (em) waves with linear polarizations parallel to the SSP waveguide due to the limitation of perpendicular grooving structures, and the polarizations of LWA radiations are difficult to arbitrarily design. We propose an efficient method to achieve the leaky-wave radiations with arbitrarily customizable polarizations based on an alternative SSPP LWA, which is made of a periodically modulated SSP waveguide with bilateral 45°-tilted grooves to generate two orthogonally polarized em waves. The grooves on both sides of the SSPP LWA can be designed with proper displacement to provide the required phase difference between two orthogonally polarized radiation waves in order to customize the polarization of the leaky-wave radiations. Both simulation and experimental results are provided to validate the feasibility of tailoring arbitrary polarizations for the radiation waves based on the proposed SSPP LWA.

DOI: 10.1103/PhysRevApplied.12.014036

I. INTRODUCTION

In the optical region, surface plasmon polaritons (SPPs) are caused by interaction between photons and electrons on the metal-air/dielectric interface [1], because the metals behave as dielectrics with negative permittivity. However, the natural SPPs do not exist when the frequency scales down to far infrared, terahertz, and microwave bands, because metals behave as perfectly electric conductors (PECs) in these frequency bands. To mimic the characteristics of extraordinary field confinements and enhancements of natural SPPs, spoof surface plasmon polaritons (SSPPs) have been designed by decorating a series of periodically artificial structures on the metal surface [2–8]. The SSPPs are not the true natural SPPs excited by electron oscillations, but it has been proven that the characteristics of SSPPs are very similar to the natural SPPs [2–4], whose electromagnetic fields decay exponentially and propagate efficiently along the directions vertical and parallel to the interface, respectively. In the past few years, SSPP devices have been widely investigated and have shown extraordinary potential in many areas in which SSPPs-based leaky-wave antennas (LWAs) are noteworthy due to their advantages of miniaturization, low profile, and easy fabrication [9–22]. However, in previous works, the polarizations of leaky-wave radiations are naturally parallel to the LWAs in most cases due to the perpendicular grooving structures [9–18]. Only a few circularly polarized SSPP LWAs are realized by using SSPPs as feeding networks rather than the source of the circularly polarized radiation [19–21]. Hence, current SSPP LWAs are not flexible enough in situations where multiple polarized radiation is needed, such as satellite communications and personal terminals.

In this paper, a simple method has been presented to realize the arbitrarily customizable polarization of radiation waves based on SSPP LWA, and the basic idea is to construct a pair of perpendicular radiation electric fields with the same amplitude and customizable phase difference. A bilateral slotted SSP waveguide composed of 45°-tilted grooves on both sides is proposed and any pair of tilted grooves on both sides are perpendicular to each other. By controlling the groove depth of each unit, the surface impedances of the SSP waveguide is designed to be sinusoidal modulation, so the propagating SSPPs can be converted to leaky-wave radiations [22–24]. Due to the mutually perpendicular slots on both sides, the electric fields of radiation waves generated by the different sides are perpendicular to each other with the same amplitude. Hence, the polarization of leaky waves completely depends on the phase difference between these two orthogonal electric fields, which can be customized by changing the relative displacement of grooves on both sides of the SSPP LWA. The simulation results show that the leaky-wave radiations with arbitrarily desired polarization can be easily achieved by the proposed SSPP LWA with

*hfma@seu.edu.cn

bilateral tilted grooves, in which the cases of horizontally, perpendicularly, and circularly polarized radiation have been further verified by experiments, showing good performance.

II. THEORETICAL ANALYSIS

In most existing literature on SSPPs, the unit cells are either the unilateral perpendicular slotting structure shown as a "perpendicular unit" in Fig. 1(a) [7] or the bilateral perpendicular slotting structure that is the reverse combination of two unilateral slotting structures [25]. In fact, the dispersion characteristics of these two kinds of SSPP units (unilateral or bilateral) are almost consistent with each other if they have the same groove depths [25]. However, SSPP LWAs composed of these structures, no matter whether with a unilateral or bilateral unit, can only support linearly polarized waves [11,13].

Here, we modify the perpendicular slotting unit to a 45°-tilted one shown as the "tilted unit" in Fig. 1(b), in which $d = 1.7$ mm, $a = 0.7d$, $H = 6$ mm, and h is variable. The simulated dispersion curves of units with varied h are shown in Fig. 1(c), which indicates that the propagating wave number k_x increases with the increase of h. In addition, according to Maxwell equations, the surface impedance η_{surf} can be calculated once k_x is achieved [26,27]

$$\eta_{\text{surf}} = j\,\eta_0\sqrt{n_s^2 - 1}, \tag{1}$$

where $\eta_0 = \sqrt{\mu_0/\varepsilon_0}$ is the wave impedance in free space, j is the imaginary unit, and n_s is the effective mode index of the surface wave calculated as

$$n_s = k_x c/2\pi f_0, \tag{2}$$

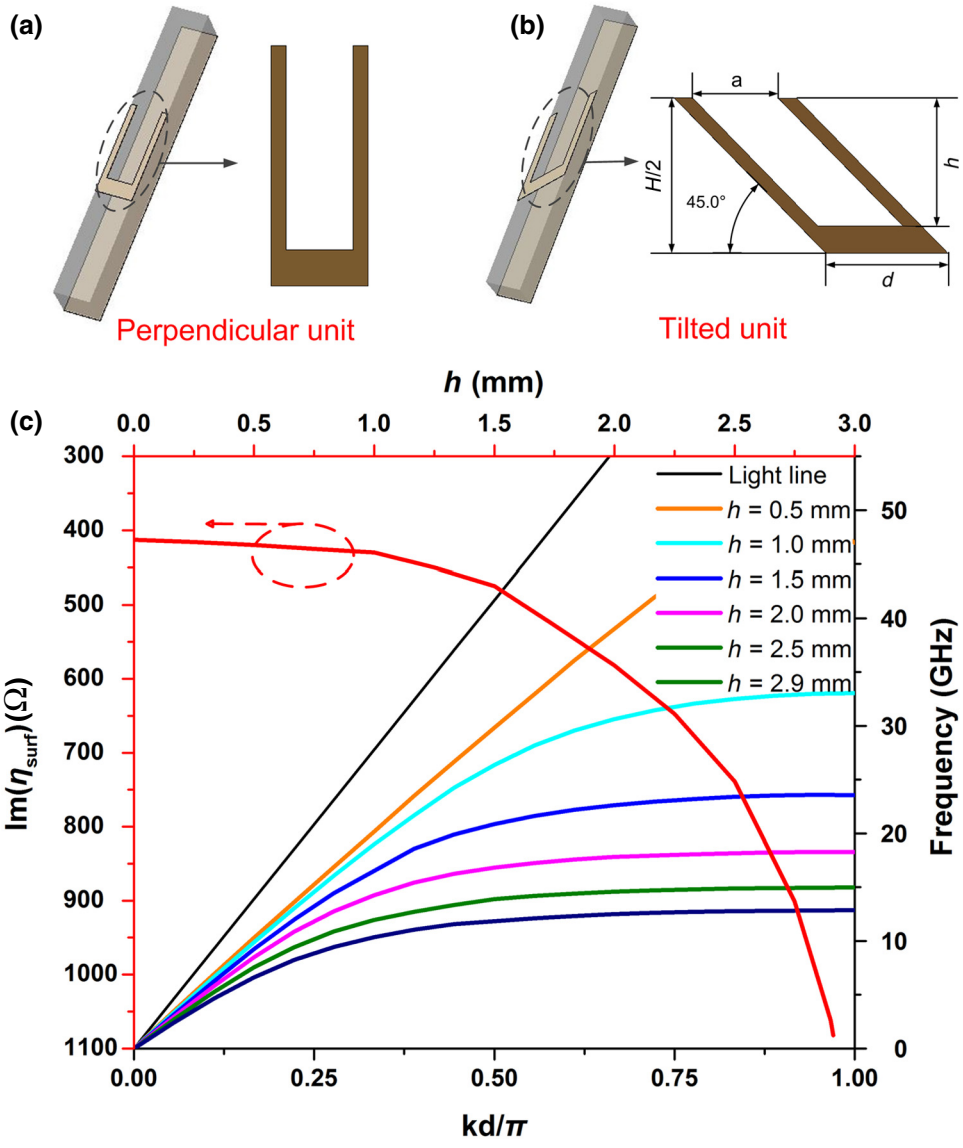

FIG. 1. SSPP unit cells and dispersion curves. (a) Perpendicular unit. (b) The proposed tilted unit. (c) Dispersion curves and surface impedance of tilted unit with different groove depths h at 9 GHz.

in which c is the velocity of light in free space and f_0 is the working frequency. The calculated surface impedances with different h at 9 GHz are also given in Fig. 1(c) with the red solid line.

Figure 2 illustrates the schematic of the designed SSPP LWA, which is printed on a grounded dielectric substrate of F4BK225 with a relative permittivity of 2.25, loss tangent of 0.001, and thickness of 2 mm. It is worth mentioning that the F4BK225 is a kind of common commercial polytetrafluoroethylene (PTFE) resin-based dielectric substrate, which is widely used in the standard printed circuit board (PCB) fabrication process due to its low cost and stable electrical performance. The SSPP LWA is composed of bilateral 45°-tilted slotting structures in which any pairs of grooves on the same cross section are perpendicular to each other. To convert SSPPs to leaky-wave radiations, the surface impedance of the SSPP LWA should be periodically modulated by decorating the grooves with different depths [14]. Here, we choose the sinusoidal periodic modulation

$$\eta_{\mathrm{surf}}(x) = jX_s\left[1 + M\cos\left(\frac{2\pi x}{P}\right)\right], \tag{3}$$

in which X_s is the average surface impedance, M is the modulation factor, and P is the modulation period. Then the radiation angle of leaky waves away from the broadside can be calculated by [22]

$$\theta = \mathrm{arc}\ \sin\left(\sqrt{1+X'^2} - \frac{2\pi}{k_0 P}\right), \tag{4}$$

where $X' = X_s/\eta_0$ is the average surface reactance normalized by the free-space wave impedance (η_0) and k_0 is the free-space wave number at designed frequency f_0. The X_s and M can be achieved by

$$X_s = \frac{Z_{s1} + Z_{s2}}{2}, \tag{5}$$

$$M = \frac{|Z_{s1} - Z_{s2}|}{2X_s}, \tag{6}$$

where Z_{s1} and Z_{s2} are the maximum and the minimum surface impedances of the unit within one period, respectively. According to Eq. (4), the radiation angle of leaky waves can be completely determined by the period of P and average surface impedance of X'.

The proposed SSPP LWA is composed of 16 modulation periods with a period of $P = 17$ mm, as shown in Fig. 2, which is connected to two grounded coplanar waveguides (CPWs) with 50 ohms on the input and output ports [8], and the total length of the LWA is 311.65 mm. We arbitrarily choose $\theta = 16.5°$ as a radiation direction of leaky waves at 9 GHz, then the $X' = 2.01$ and $X_s = \eta_0 X' = 758\ \Omega$ can be calculated from Eq. (4). According to Fig. 1(c), the surface impedance of the unit with different groove depths is varied from 413 to 1082 Ω at 9.0 GHz when the depth of each cell h increases from 0 to 2.91 mm. In order to achieve high-radiation efficiency, the modulation factor of M must as large as possible to cover the range of surface impedance with different groove depths [14], so we chose $Z_{s1} = 433\ \Omega$ with $h = 1.1$ mm and $Z_{s2} = 1082\ \Omega$ with $h = 2.91$ mm to simultaneously guarantee maximum $M = 0.43$ and the required $X_s \approx 758\ \Omega$. Substituting P, M, and X_s into Eq. (1), the surface impedance along the propagating direction (x axis) can be calculated, and then the groove depths (h) of each unit of the sinusoidal-modulated SSPP LWA can be achieved according to the relationship between the surface impedance η_{surf} and the groove depth h. Those of the final designed LWA are demonstrated in Fig. 2. It should be mentioned that the surface

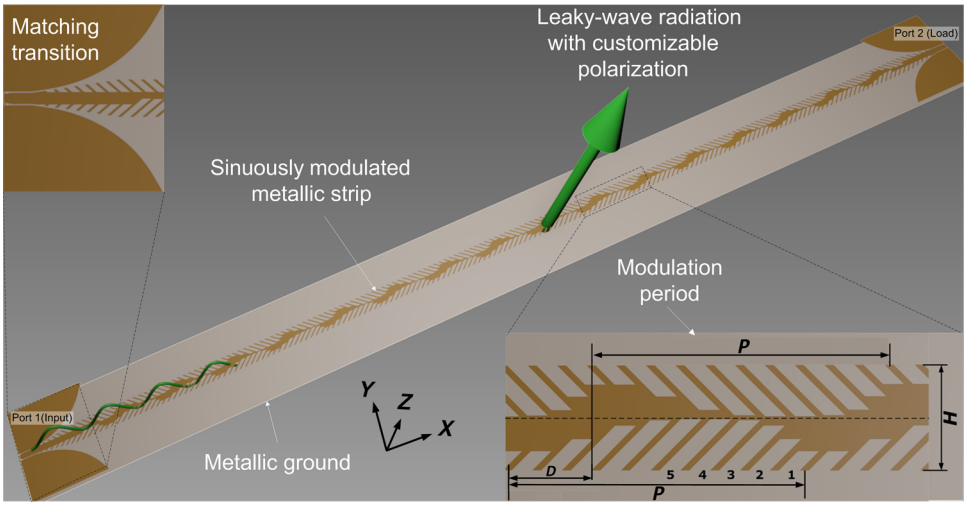

FIG. 2. Schematic of the SSPP LWA composed of tilted units.

TABLE I. The depth of each cell and related surface impedance.

No.	1	2	3	4	5
h (mm)	1.1	1.78	2.55	2.87	2.91
Im(η_{surf}) (ohm)	433	532	756	1005	1082

impedance modulations on both sides of the SSP waveguide have the same modulation period (P), average surface impedance (X_s), and modulation factor (M), but have a relative shift of D. One of the modulated periods is enlarged at the lower right corner of Fig. 2 and each modulated period is composed of 10 units. The final groove depths and corresponding surface impedances of the units in the half periods marked as 1, 2, 3, 4, 5 in the inset of Fig. 2 are listed in Table I. Figure 3 shows the full-wave simulated electric field distributions on the top layer of the proposed SSPP LWA at 9.0 GHz, which demonstrates that two orthogonal electric field components of leaky-wave radiations are provided by each side of 45°-tilted grooves, so the polarization of the radiations only depends on the phase differences ($\Delta\varphi$) between these two orthogonal electric fields, which can be achieved by changing the relative displacement of D between both sides of SSPP LWA.

III. NUMERICAL SIMULATIONS

Three specific examples are given to verify the feasibility of polarization customization for leaky-wave radiations, and the simulated results are provided to validate the theoretical expectation. In designing, we assume that the $+y$ side of LWA remains unmoved, but the $-y$ side of LWA can be designed to horizontal shift with a displacement of D, which is a positive or negative value when the $-y$ side shifts to the left or right, respectively. The signals are fed from the left port (Port 1) of SSPP LWA.

When $D = 0$, that is, there is no relative shift between both sides, and the LWA is a symmetrical structure, the two radiated orthogonal electric fields have a phase difference of $\Delta\varphi = 0$, and then the radiation waves generated by the SSPP LWA will be x polarized waves with the electric fields parallel to LWA. Figure 4(a) illustrates the simulated near-field distributions of electric fields in the x-o-z plane at 9 GHz, which shows that SSPPs are completely converted to x polarized radiation waves without the component of E_y. Figure 4(b) illustrates the simulated far-field patterns of E_x (horizontal polarization) and E_y (perpendicular polarization), which validate that the radiation waves are linearly polarized (x polarized) waves with a high cross-polarization level over 40 dB.

When D is increased to 4.83 mm, which is about $\lambda_g/4$ of SSPPs (λ_g is the wavelength of SSPPs) at 9 GHz, the phase difference of the two radiated orthogonal electric fields is changed to 90°, and then the radiation waves will be circularly polarized waves. Figure 5(a) illustrates the radiated near-field distributions of E_x and E_y, which show that the amplitudes of E_x and E_y are nearly the same but E_y is 90° ahead of E_x in phase. Figure 5(b) illustrates the simulated far-field radiation patterns, indicating that the radiation waves are purely left-handed circularly polarized (LHCP) waves with a high cross-polarization level over 20 dB.

When D is further increased to 9.66 mm, which is about $\lambda_g/2$ of SSPPs at 9 GHz, the phase difference of the two radiated orthogonal electric fields will be changed to 180°, and then the radiation waves will be y polarized waves. Figure 6(a) illustrates the simulated near-field distributions of E_x and E_y, showing that SSPPs are converted to y polarized radiation waves without the E_x component. The simulated far-field radiation patterns also demonstrate

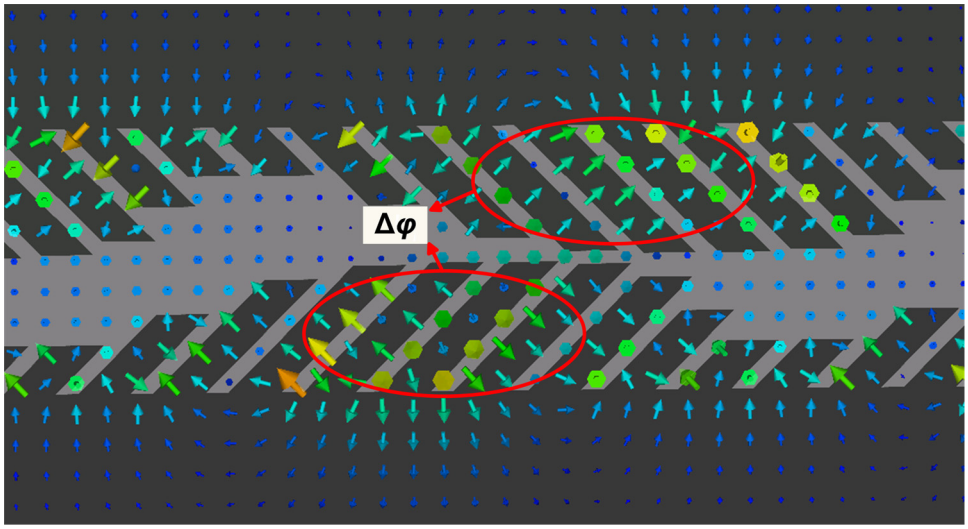

FIG. 3. Full-wave simulated electric field distributions on the top layer of the proposed SSPP LWA at 9.0 GHz.

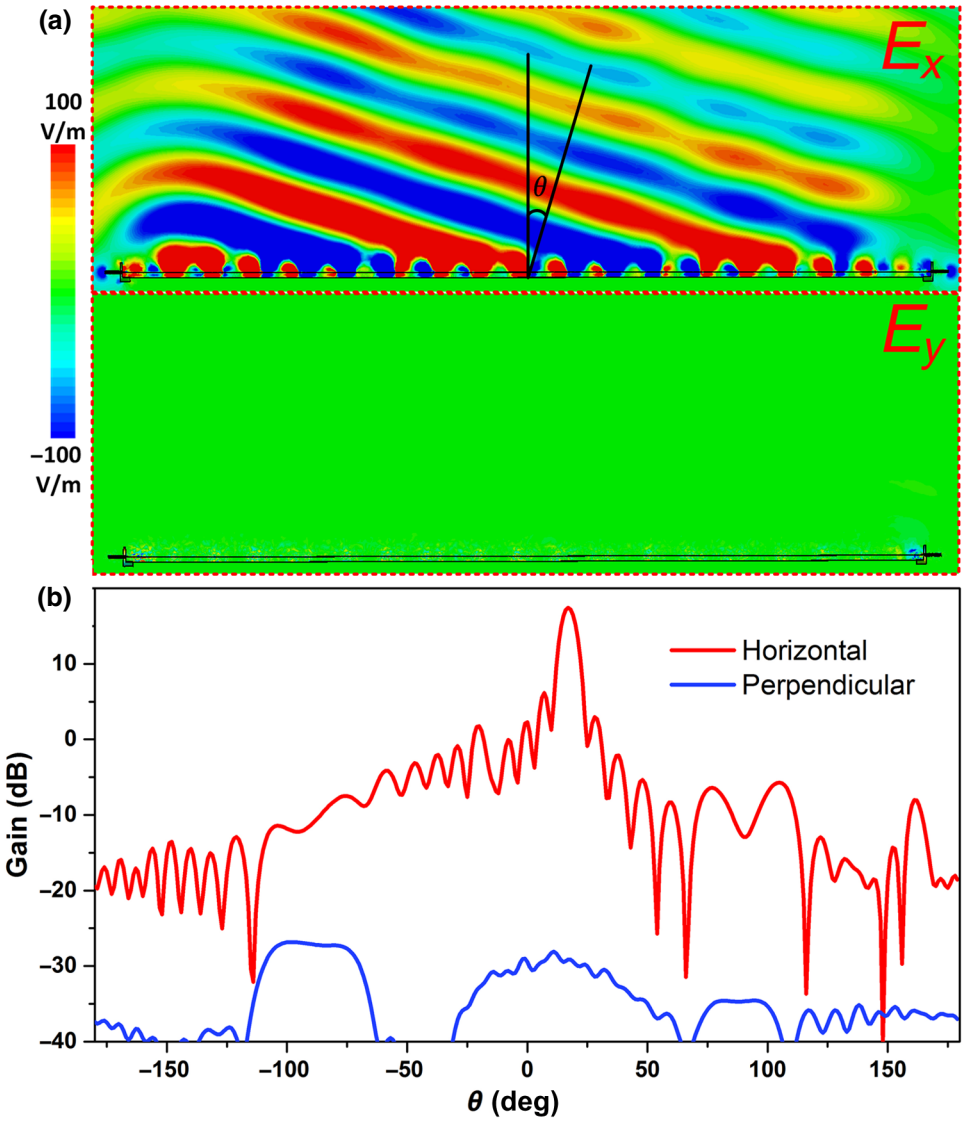

FIG. 4. Comparison between horizontal and perpendicular polarization at 9.0 GHz when $D = 0$ mm. (a) Simulated near-field distributions of E_x and E_y in the x-o-z plane. (b) Simulated far-field radiation patterns in the x-o-z plane.

that the radiation waves are linearly polarized (y polarized) waves, as shown in Fig. 6(b).

So far, the x polarized, LHCP, and y polarized radiation waves have been realized by changing the displacement D to obtain different phase differences $\Delta\varphi$. Actually, the arbitrary polarization can be realized by changing the displacement D, such as right-handed circular polarization (RHCP), elliptical polarization, and so on, which has been summarized in Table II. In addition, the radiation angle of the beam at a fixed frequency can be controlled by changing the modulation period P or average surface impedance X_s according to Eq. (3).

It should be mentioned that the simulated directions (θ_{sim}) of leaky-wave radiations are 16.5°, 12°, and 7° when $D = 0$, 4.83, and 9.66 mm, respectively, as shown in Figs. 4(b), 5(b), and 6(b), which are not very consistent with the designed angle of $\theta_{\text{des}} = 16.5°$, showing the larger the displacement of D, the larger the angle error ($\theta_{\text{simerr}} = \theta_{\text{des}} - \theta_{\text{sim}}$). The simulated angle errors (θ_{simerr}) with the change of D between the full-wave simulations and designed angle ($\theta_{\text{des}} = 16.5°$) are summarized and illustrated in Fig. 7 with the black solid line. The results show that the errors increase with the increase of D, and the maximum error is 9.6° when $D = \pm 9.66$ mm. The cause of the errors is the relative shift of the tilted grooves on both sides of LWAs, and then the effective mode index (n_s) of the LWA slightly changes, resulting in the radiation angle error. According to Eqs. (1)–(4), when the radiation angle is designed to be $\theta_{\text{des}} = 16.5°$, the required effective mode index of LWA should be $n_{\text{des}} \approx 2.25$. However, if the SSPP LWA is designed unsymmetrically with a relative shift between both sides, then the actual effective mode indices (n_s) of the LWAs will change accordingly. The actual n_s of the LWAs with a different displacement of D can be calculated from the S parameter retrieval methods [28,29], which are illustrated in Fig. 7 with the blue solid

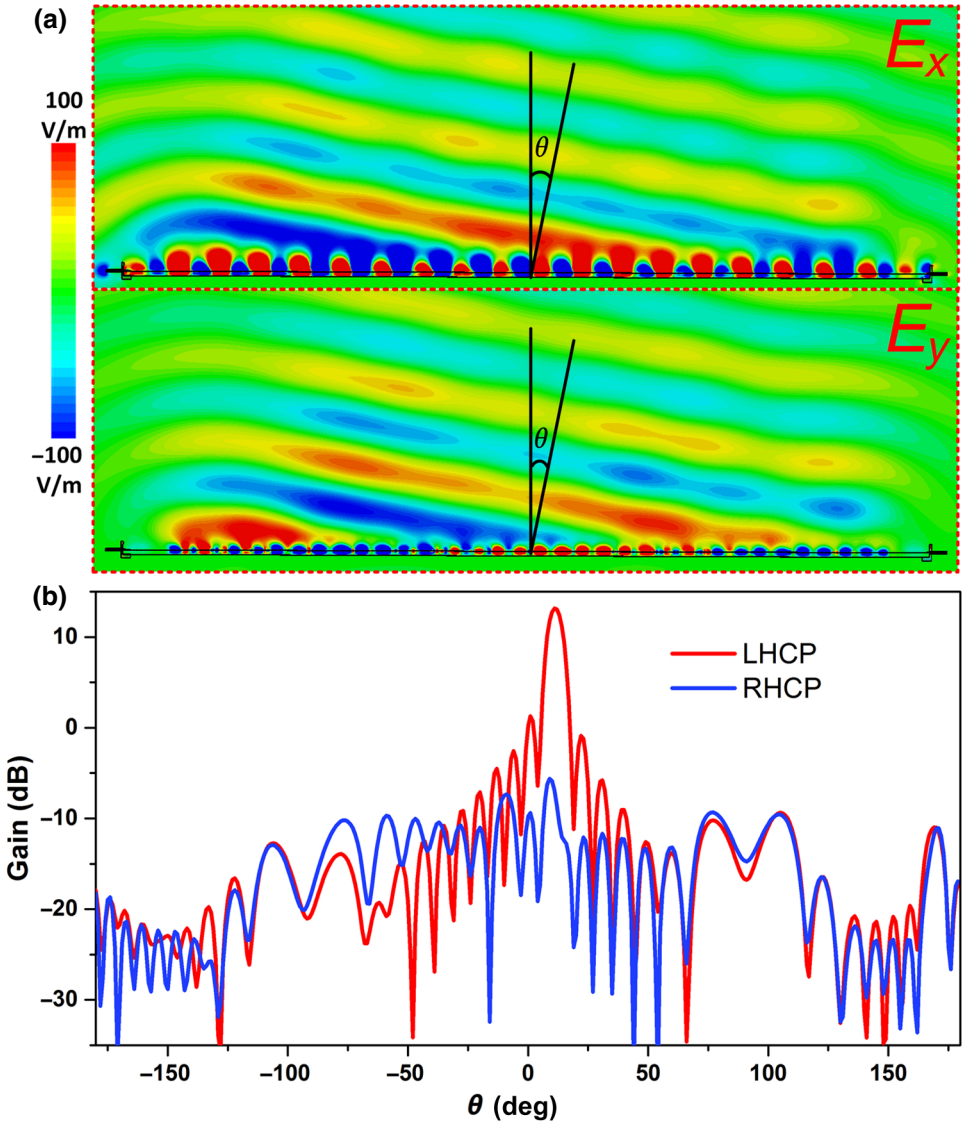

FIG. 5. Comparison between LHCP and RHCP at 9.0 GHz when $D = 4.83$ mm. (a) Simulated near-field distributions of E_x and E_y in the x-o-z plane. (b) Simulated far-field radiation patterns in the x-o-z plane.

line. Based on the retrieved n_s, the calculated radiation angles (θ_{cal}) of beams with different D can be recalculated by using Eqs. (1)–(6), and the calculated angle errors ($\theta_{\text{calerr}} = \theta_{\text{des}} - \theta_{\text{cal}}$) are also illustrated in Fig.7 with the black dashed line, which are quite consistent with the calculated errors of θ_{simerr}. Hence, we can conclude that the angle errors are mainly caused by the change of effective mode index due to the relative shift of grooves on both sides of the LWAs.

IV. EXPERIMENTAL MEASUREMENTS

To further verify our design in experiment, three typical LWAs based on the designed SSPP waveguide with $D = 0$, 4.83, and 9.66 mm are fabricated by using the standard PCB fabrication process.

Figure 8(a) shows a photograph of the fabricated SSPP LWA with $D = 0$ mm. The measured S parameters have good agreement with the simulations as illustrated in Fig. 8(b), which show that the $S11$ is less than -10 dB and $S21$ is less than -8.5 dB, indicating high radiation efficiency of the SSPP LWA. Figure 8(c) shows the measured normalized far-field radiation patterns in the x-o-z plane. As expected, the radiations are x polarized waves with effective cross-polarization suppression, which have a good agreement with the simulated results shown in Fig. 4(b). In addition, the main beam scans from 15.1° to 36.5° as the frequency increases from 9 to 10 GHz, showing the natural frequency scanning characteristics of LWAs [22].

Figure 9(a) shows a photograph of the fabricated SSPP LWA with $D = 4.83$ mm. Both simulated and measured S parameters have a good agreement with each other as illustrated in Fig. 9(b). The reflection coefficients of S_{11} and transmission coefficients of S_{21} are less than -10 dB and -7.5 dB, respectively, in a broad band

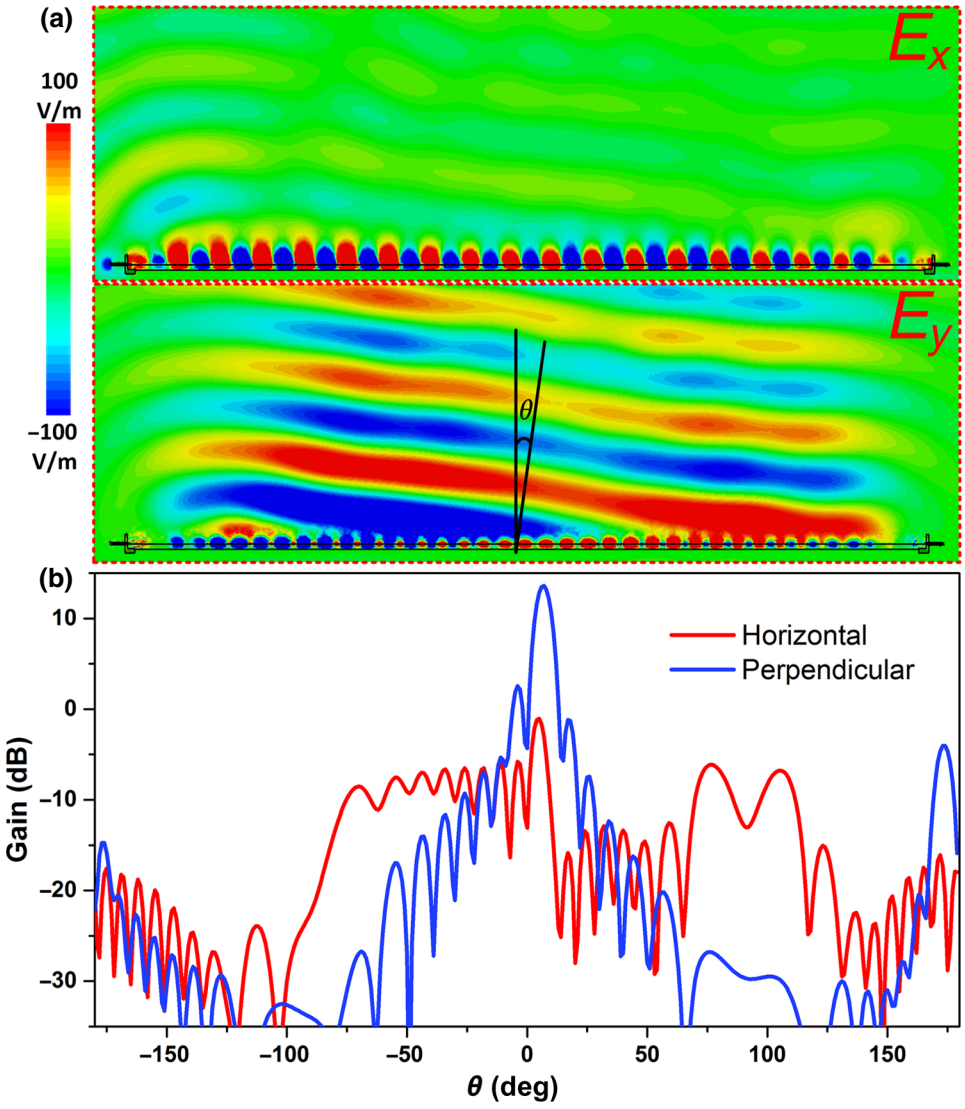

FIG. 6. Comparison between horizontal and perpendicular polarization at 9.0 GHz when $D = 9.66$ mm. (a) Simulated near-field distributions of E_x and E_y in the x-o-z plane. (b) Simulated far-field radiation patterns in the x-o-z plane.

from 8.7 to 10.0 GHz, which indicates that the most of input power is also radiated into free space. In addition, the axial ratios of radiation beams are also illustrated in Fig. 9(b), which are below 3 dB from 8.7 to 10.0 GHz as demonstrated in Fig. 9(b), to show good circularly polarized characteristics of leaky waves in a wide frequency range. Figure 9(c) illustrates the measured normalized far-field radiation patterns of the SSPP LWA in the x-o-z plane, showing that the principal- and cross-polarizations are LHCP and RHCP, respectively, which have a good agreement with the simulated results shown in Fig. 5(b). In addition, the main beam also scans from 11.2° to 32.2° as frequencies increase from 9 to 10 GHz. It is worth mentioning that the axis ratio of the radiation beams achieved in this work is about 2 dB, which is larger than that of 0 dB for an ideal circular polarization. The reason for this is because the relative shift of grooves on both sides of the LWAs results in the slight difference between the orthogonal amplitude components of radiation waves. Actually, the ideal 0 dB axis ratio

TABLE II. The polarization of the leaky-wave radiation varies with D.

D (mm)	−9.66	−7.24	−4.83	−2.41	0	2.41	4.83	7.24	9.66
$\Delta\varphi$ (degree)	−180	−135	−90	−45	0	45	90	135	180
Polarization	↑				→				↓

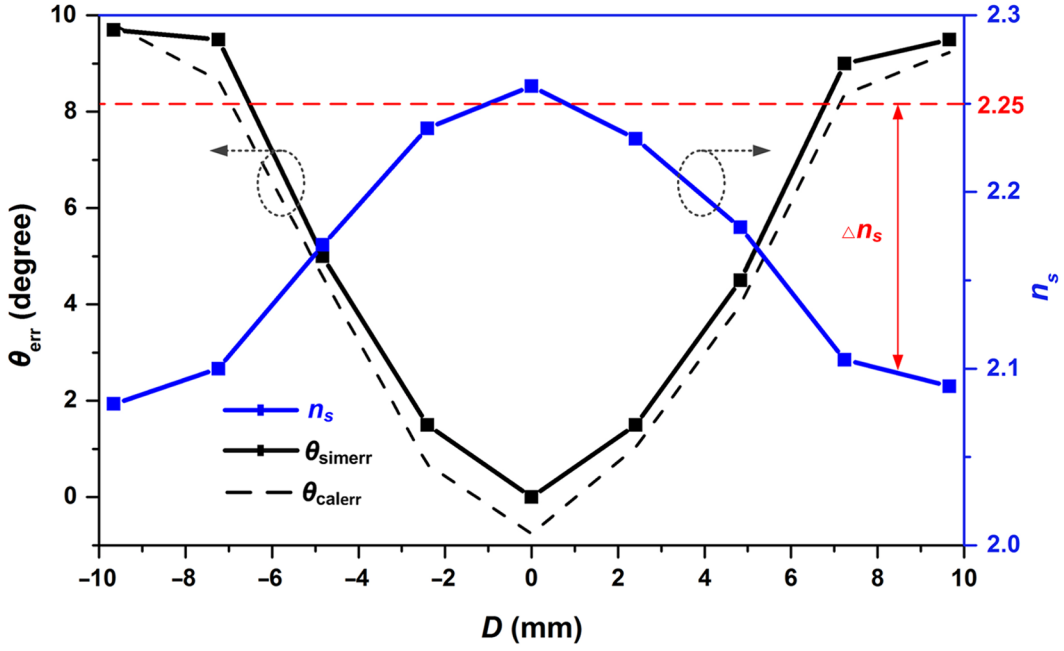

FIG. 7. The effective mode index (n_s) and beam direction errors (θ_{calerr} and θ_{simerr}) vary with D at 9.0 GHz.

is very difficult to achieve in practical applications, and the beams can be approximatively considered as a circular polarization only if the axial ratio is less than 3 dB [19–21,30–32].

Figure 10(a) shows a photograph of the fabricated SSPP LWA with $D = 9.66$ mm. The simulated and measured $S11$ and $S21$ are also consistent with each other as illustrated in Fig. 10(b), in which some mismatches of curves are caused by the experimental and measurement errors. In addition, the measured normalized far-field radiation patterns are illustrated in Fig. 10(c), and the y polarized radiation waves are achieved as expected, which have a good

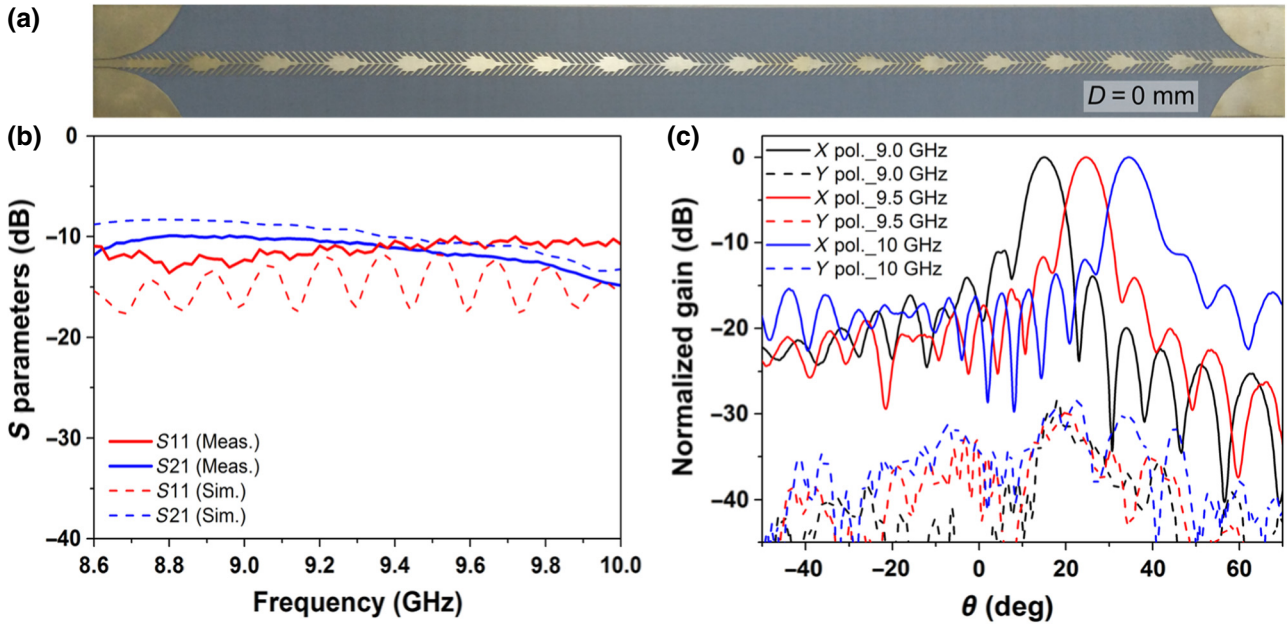

FIG. 8. The simulated and measured results of SSPP LWA with $D = 0$ mm. (a) Photograph of the fabricated SSPP LWA. (b) S parameters. (c) Measured normalized far-field radiation patterns.

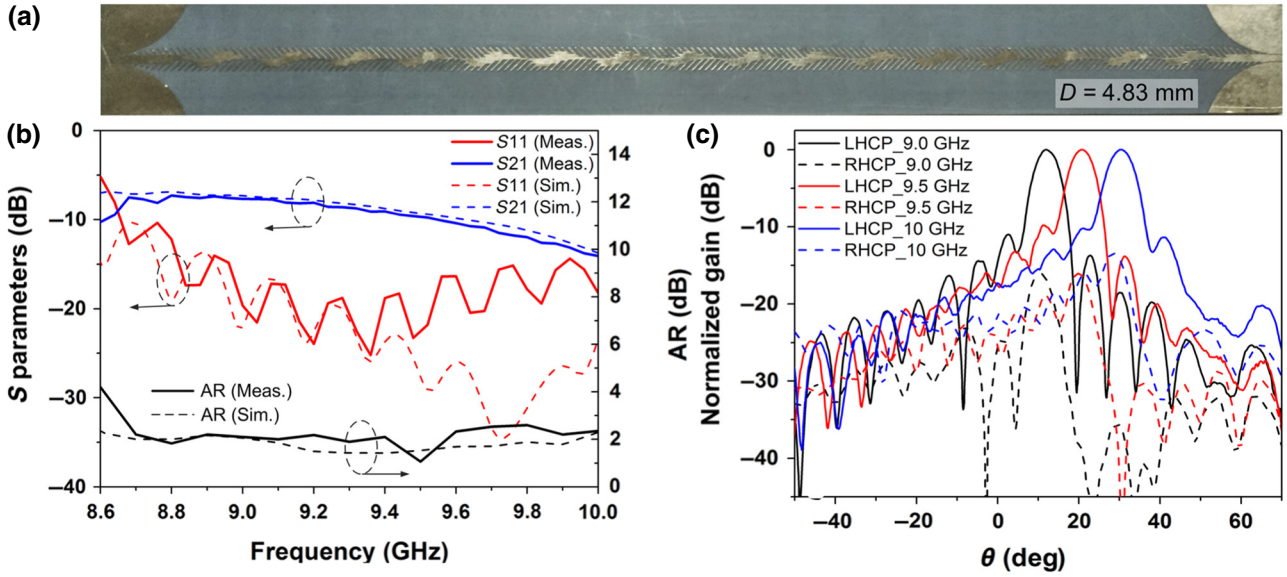

FIG. 9. The simulated and measured results of SSPP LWA with $D = 4.83$ mm. (a) Photograph of the fabricated SSPP LWA. (b) S parameters and axial ratios. (c) Measured normalized far-field radiation patterns.

agreement with the simulated results shown in Fig. 6(c). In addition, the radiation beam scans from 5.1° to 24.9° as the frequency changes from 9 to 10 GHz.

Figure 11(a) shows the simulated and measured gains of the SSPP LWAs as the frequency changes from 9 to 10 GHz and both simulated and measured results have a good agreement with each other, all of which are larger than 12 dB. The simulated radiation and total efficiencies of the LWAs are provided in Fig. 11(b). The radiation efficiencies vary from 69% to 72%, 62% to 74%, and 58% to 77%, and the total efficiencies vary from 58% to 62%, 48% to 66%, and 47% to 71% for x, circular- and y polarized SSPP LWAs, respectively, as frequency increases from 9 to 10 GHz.

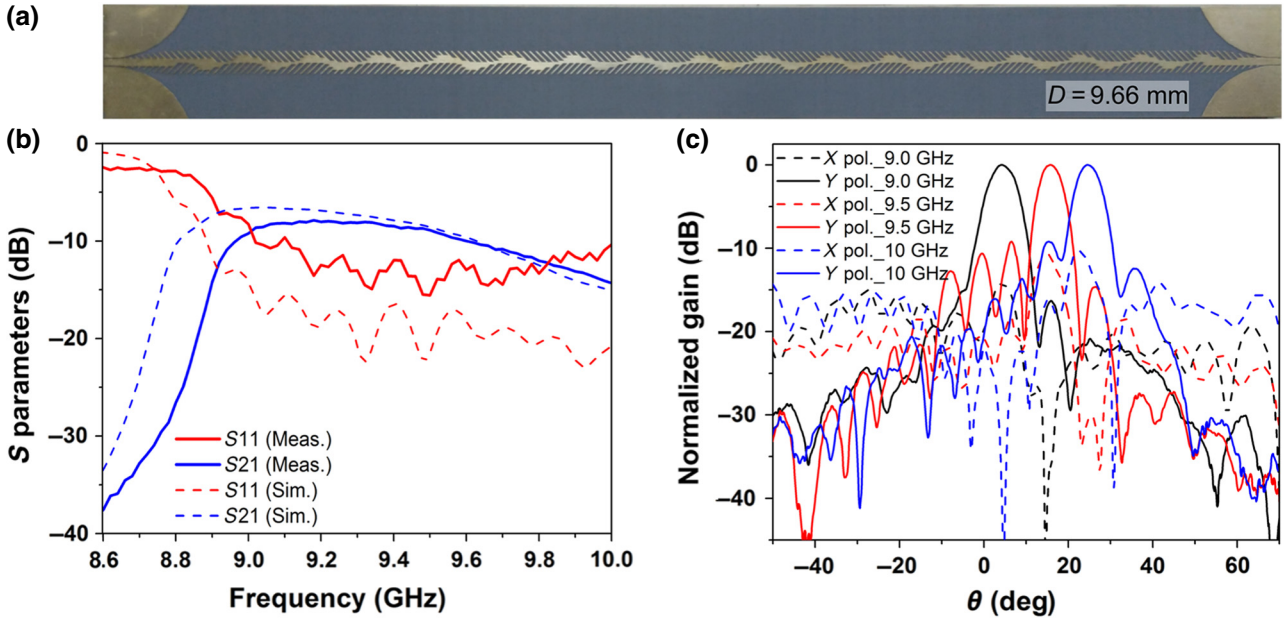

FIG. 10. The simulated and measured results of SSPP LWA with $D = 9.66$ mm. (a) Photograph of the fabricated SSPP LWA. (b) S parameters. (c) Measured normalized far-field radiation patterns.

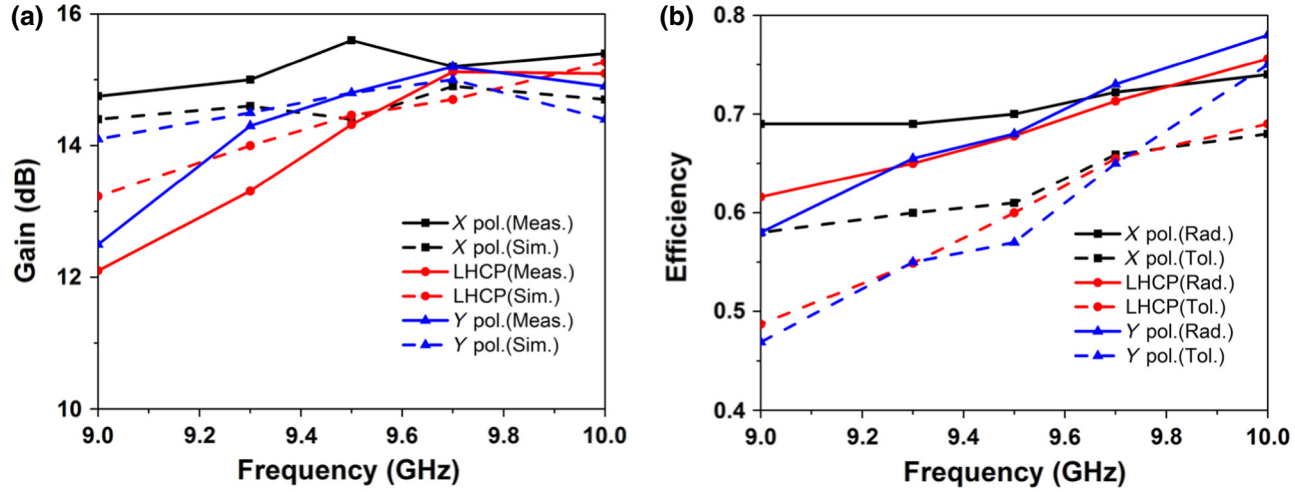

FIG. 11. The gains and radiation efficiencies. (a) The simulated and measured gains. (b) The simulated radiation and total efficiencies.

V. CONCLUSION

A simple method has been presented to customize arbitrary polarizations of the leaky-wave radiations based on a periodically modulated SSP waveguide. A modified unit with a 45°-tilted groove has been proposed to construct the SSPP LWA, which is a bilateral tilted slotting structure with grooves on both sides perpendicular to each other. The surface impedances of LWAs on both sides are sinusoidally modulated with the same period, average surface impedance, and modulation factor, so the waves radiated by each side of the LWA are directed to the same direction with the same amplitude, but the electric fields are orthogonal. By making a relative shift of grooves on both sides of the LWA, the arbitrary phase difference between two orthogonal electric fields can be achieved, and then the polarization of radiation waves can be customized by designing the required phase difference. The horizontal, circular, and perpendicular polarizations are verified by both simulations and experiments to validate the theoretical expectations, which show a good agreement with each other.

ACKNOWLEDGMENTS

This work was supported by the National Key Research and Development Program of China (Grants No. 2017YFA0700201, No. 2017YFA0700202, and No. 2017YFA0700203), National Natural Science Foundation of China (Grants No. 61831006, No. 61522106, No. 61571117, No. 61501117, No. 61501112, No. 61631007, and No. 61701107), and the 111 Project (Grant No. 111-2-05).

M. W. and H. F. M. contributed equally to this work.

[1] W. L. Barnes, A. Dereuxand, and T. W. Ebbesen, Surface plasmon subwavelength optics, Nature **424**, 824 (2003).

[2] J. B. Pendry, L. Martin-Moreno, and F. J. Garcia-Vidal, Mimicking surface plasmons with structured surfaces, Science **305**, 847 (2004).

[3] F. J. Garcia-Vidal, L. Martin-Moreno, and J. B. Pendry, Surfaces with holes in them: new plasmonic metamaterial, J.Opt. A Pure Appl. Opt. **7**, S97 (2005).

[4] A. P. Hibbins, B. R. Evans, and J. R. Sambles, Experimental verification of designer surface plasmons, Science **308**, 670 (2005).

[5] S. A. Maier, S. R. Andrews, L. Martin-Moreno, and F. J. Garcia-Vidal, Terahertz Surface Plasmon-Polariton Propagation and Focusing on Periodically Corrugated Metal Wires, Phys. Rev. Lett. **97**, 176805 (2006).

[6] P. Nagpal, N. C. Lindquist, S. H. Oh, and D. J. Norris, Ultrasmooth patterned metals for plasmonics and metamaterials, Science **325**, 594 (2009).

[7] X. Shen, T. J. Cui, D. Martin-Cano, and F. J. Garcia-Vidal, Conformal surface plasmons propagating on ultrathin and flexible films, Proc. Natl Acad. Sci. USA **110**, 40 (2013).

[8] Z. X. Xu, X. X. Yin, and D. F. Sievenpiper, Adiabatic Mode-Matching Techniques for Coupling Between Conventional Microwave Transmission Lines and One-Dimensional Impedance-Interface Waveguides, Phys. Rev. Appl. **11**, 044071 (2019).

[9] O. Quevedo-Teruel, Controlled radiation from dielectric slabs over spoof surface plasmon waveguides, Prog. Electromagn. Res. **140**, 169 (2013).

[10] A. K. Klein, A. Basden, J. Hammler, L. Tyas, M. Cooke, C. Balocco, D. Zeze, J. M. Girkin, and A. Gallant, Scattering of spoof surface plasmon polaritons in defect-rich THz waveguides, Sci. Rep. **9**, 6288 (2019).

[11] A. Kianinejad, Z. N. Chen, and C. W. Qiu, A single-layered spoof-plasmon-mode leaky wave antenna with consistent gain, IEEE Trans. Antennas Propag. **65**, 681 (2017).

[12] Y. J. Han, J. F. Wang, S. H. Gong, Y. F. Li, Y. Zhang, and J. Q. Zhang, Low RCS antennas based on dispersion engineering of spoof surface plasmon polaritons, IEEE Trans. Antennas Propag. **66**, 7111 (2018).

[13] M. R. Tavakol, A. Saba, K. Arik, and A. Khavasi, Tunable leaky-wave radiation by graphene-covered corrugated surfaces, Appl. Opt. **57**, 8971 (2018).

[14] A. H. Panaretos and D. H. Werner, Spoof plasmon radiation using sinusoidally modulated corrugated reactance surfaces, Opt. Express **24**, 2443 (2016).

[15] A. Kandwal, Q. F. Zhang, X. L. Tang, L. W. Liu, and G. Zhang, Low-profile spoof surface plasmon polaritons traveling-wave antenna for near-endfire radiation, IEEE Antennas Wirel. Propag. Lett. **17**, 184 (2018).

[16] Y. Fan, J. F. Wang, Y. F. Li, J. Q. Zhang, S. B. Qu, Y. J. Han, and H. Y. Chen, Frequency scanning radiation by decoupling spoof surface plasmon polaritons via phase gradient metasurface, IEEE Trans. Antennas Propag. **66**, 203 (2018).

[17] X. L. Tang, Q. F. Zhang, S. M. Hu, S. K. Ge, Y. F. Chen, and H. Yu, Beam Steering Using Momentum-Reconfigurable Goubau Meta-Line Radiators, Sci. Rep. **8**, 11854 (2018).

[18] Y. J. Han, Y. F. Li, H. Ma, J. F. Wang, D. Y. Feng, S. B. Qu, and J. Q. Zhang, Multibeam antennas based on spoof surface plasmon polaritons mode coupling, IEEE Trans. Antennas Propag. **65**, 1187 (2017).

[19] X. M. Lv, W. Q. Cao, Z. Y. Zeng, and S. J. Shi, A circularly polarized frequency beam-scanning antenna fed by a microstrip spoof SPP transmission line, IEEE Antennas Wirel. Propag. Lett. **17**, 1329 (2018).

[20] Q. L. Zhang, Q. F. Zhang, and Y. F. Chen, High-efficiency circularly polarised leaky-wave antenna fed by spoof surface plasmon polaritons, IET Microw. Antenna Propag. **12**, 1639 (2018).

[21] D. F. Guan, P. You, Q. F. Zhang, Z. H. Lu, S. W. Yong, and K. Xiao, A wide-angle and circularly polarized beam-scanning antenna based on microstrip spoof surface plasmon polariton transmission line, IEEE Antennas Wirel. Propag. Lett. **16**, 2538 (2017).

[22] A. A. Oliner and A. Hessel, Guided waves on sinusoidally-modulated reactance surfaces, IRE Trans. Antennas Propag. **7**, 201 (1959).

[23] A. Epstein, J. P. S. Wong, and G. V. Eleftheriades, Cavity-excited Huygens' metasurface antennas for near-unity aperture illumination efficiency from arbitrarily large apertures, Nat. Commun. **7**, 10360 (2016).

[24] D. R. Smith, O. Yurduseven, L. P. Mancera, P. Bowen, and N. B. Kundtz, Analysis of a Waveguide-Fed Metasurface Antenna, Phys. Rev. Appl. **8**, 054048 (2017).

[25] Q. Zhang, H. C. Zhang, J. Y. Yin, B. C. Pan, and T. J. Cui, A series of compact rejection filters based on the interaction between spoof SPPs and CSRRs, Sci. Rep. **6**, 28256 (2016).

[26] J. A. Dockrey, M. J. Lockyear, S. J. Berry, S. A. R. Horsley, J. R. Sambles, and A. P. Hibbins, Thin metamaterial Luneburg lens for surface waves, Phys. Rev. B **87**, 125137 (2013).

[27] S. Maci, M. Caiazzo, A. Cucini, and M. Casaletti, A pole-zero matching method for EBG surfaces composed of a dipole FSS printed on a grounded dielectric slab, IEEE Trans. Antennas Propag. **53**, 70 (2005).

[28] X. R. Zhang, H. C. Zhang, W. X. Tang, J. F. Liu, Z. Q. Fang, J. W. Wu, and T. J. Cui, Loss analysis and engineering of spoof surface plasmons based on circuit topology, IEEE Antennas Wirel. Propag. Lett. **16**, 3204 (2017).

[29] D. R. Smith, S. Schultz, P. Markos, and C. M. Soukoulis, Determination of effective permittivity and permeability of metamaterials from reflection and transmission coefficients, Phys. Rev. B **65**, 195104 (2002).

[30] M. M. Sabahi, A. A. Heidari, and M. Movahhedi, A compact CRLH circularly polarized leaky-wave antenna based on substrate-integrated waveguide, IEEE Trans. Antennas Propag. **66**, 4407 (2018).

[31] D. Sanchez-Escuderos, M. Ferrando-Bataller, J. I. Herranz, and V. M. Rodrigo-Penarrocha, Low-loss circularly polarized periodic leaky-wave antenna, IEEE Antennas Wirel. Propag. Lett. **15**, 614 (2016).

[32] Y. L. Lyu, F. Y. Meng, G. H. Yang, D. Erni, Q. Wu, and K. Wu, Periodic SIW leaky-wave antenna with large circularly polarized beam scanning range, IEEE Antennas Wirel. Propag. Lett. **16**, 2493 (2017).